Mon. Not. R. Astron. Soc. **000**, 1–12 (2014) Printed Friday 22nd August, 2014 (MN LATEX style file v2.2)

Small carbon chains in circumstellar envelopes

R. J. Hargreaves[1⋆], K. Hinkle[2] and P. F. Bernath[1,3]
[1] *Department of Chemistry, Old Dominion University, 4541 Hampton Boulevard, Norfolk, VA 23529, USA*
[2] *NOAO, 950 North Cherry Avenue, Tucson, AZ 85719, USA*
[3] *Department of Chemistry, University of York, Heslington, York, YO10 5DD, UK*

arXiv:1408.5021v1 [astro-ph.SR] 21 Aug 2014

Accepted 19 August, 2014. Received 15 August, 2014; in original form 10 July, 2014.

ABSTRACT

Observations were made for a number of carbon-rich circumstellar envelopes using the Phoenix spectrograph on the Gemini South telescope to determine the abundance of small carbon chain molecules. Vibration-rotation lines of the ν_3 antisymmetric stretch of C_3 near 2040 cm^{-1} (4.902 μm) have been used to determine the column density for four carbon-rich circumstellar envelopes: CRL 865, CRL 1922, CRL 2023 and IRC +10216. We additionally calculate the column density of C_5 for IRC +10216, and provide an upper limit for 5 more objects. An upper limit estimate for the C_7 column density is also provided for IRC+10216. A comparison of these column densities suggest a revision to current circumstellar chemical models may be needed.

Key words: circumstellar matter – infrared: stars – individual objects: CRL 865, CRL 1922, CRL 2023, IRC +10216 – astrochemistry – molecular data.

1 INTRODUCTION

Obscured carbon stars provide us with fascinating environments to study the spectacular mass loss stage in the evolution of a typical star. In the standard model, stellar pulsation coupled with circumstellar wind ejects mass from the stellar surface into the interstellar medium. The primary consequence of stellar mass loss is the formation of a circumstellar envelope and during this process the ejected material undergoes several stages of chemical and physical processing (Olofsson 2008). The circumstellar material is made up of molecular gas and 'dusty' grains that can provide surfaces for additional processing and grain growth. As the circumstellar shell expands, photochemical processes also become important in the breakdown and formation of further molecules (Ziurys 2006).

It is well established that the carbon to oxygen (C/O) ratio dictates the molecular species in circumstellar shells due to the high stability of the CO molecule (Tsuji 1973). This allows a broad variety of molecular species to form from the remaining oxygen-rich or carbon-rich material in circumstellar shells of asymptotic giant branch (AGB) stars (Olofsson 2008). IRC +10216 (CRL 1381) is carbon-rich and is the best studied example of a circumstellar shell (Glassgold 1996; Cernicharo et al. 2010; Menten et al. 2012) with more than 80 molecules detected so far, typically from pure rotational spectra (Agúndez et al. 2012). Approximately 80% of these molecules are carbon containing species (Ziurys 2006), although an interesting oxygen chemistry has also been shown to exist (Agúndez & Cernicharo 2006), thus making circumstellar shells a challenging environment for physical and chemical models (Cherchneff 2012).

The smallest pure carbon chains (C_2 and C_3) are ubiquitous throughout the interstellar medium (Ádámkovics et al. 2003) and have been detected in diffuse interstellar clouds (Souza & Lutz 1977; Cernicharo et al. 2000), comets (Ehrenfreund & Charnley 2000) and star forming cores (Mookerjea et al. 2012). Pure carbon chains do not possess a permanent dipole moment and therefore have no allowed pure rotational transitions. A thick 'dusty' circumstellar shroud means there is little flux in the

⋆ E-mail: rhargrea@odu.edu

visible region and absorptions from electronic transitions cannot be observed due to scattering. However, this makes circumstellar envelopes ideal for observing vibration-rotation bands or low-lying electronic transitions in the infrared. The C_2 (Crampton et al. 1975), C_3 (Hinkle et al. 1988) and C_5 (Bernath et al. 1989) pure carbon chains have been detected in IRC +10216. Longer pure carbon chains have yet to be identified but their derivatives, such as HC_n ($n = 1-8$), H_2C_n ($n = 2-4$) and $HC_{2n}N$ ($n = 1-5$,) are prominent species in circumstellar shells and interstellar clouds (Ehrenfreund & Charnley 2000). Small carbon chains (C_n) are therefore believed to be the fundamental building blocks of larger carbon containing species, such as polycyclic aromatic hydrocarbons (PAHs), cyanopolyynes and fullerenes (Ehrenfreund & Charnley 2000; Kaiser 2002). Indeed, the pure carbon molecules, C_{60} and C_{70}, have been observed in planetary nebulae (Cami et al. 2010). Small carbon chains are also important in flame chemistry (Baronavski & McDonald 1977) and soot formation (Goulay et al. 2010).

Understanding circumstellar chemistry relies heavily on the archetypical object IRC +10216 due to its proximity and large mass loss (Olofsson 2008; Agúndez et al. 2012). Spectral surveys have been preformed on circumstellar shells around other carbon stars, such CIT 6 (Zhang et al. 2009a) and CRL 3068 (Zhang et al. 2009b), which both show a similar chemical composition to IRC +10216. However, as a carbon-rich AGB star evolves, the chemical composition changes primarily due to photochemical processes (Cernicharo et al. 2011). The circumstellar winds transport molecules and dust into the envelope where chemical pathways are thought to lead to the formation of carbon chains and aromatic rings (Cherchneff 2006, 2012). These molecules are then broken down as a part of the AGB shell evolution towards planetary nebulae. Determining the abundance of small chains in circumstellar shells allow chemical models to be refined, whilst comparing carbon chain abundances between carbon-rich circumstellar shells determines the appropriateness of IRC +10216 as the prototypical example.

Vibration-rotation transitions of pure carbon chains allow the detection of these molecules in circumstellar envelopes when high-resolution experimental data is available. The ν_3 antisymmetric stretch of C_3 has been the focus of a number of experimental and theoretical studies (Matsumura et al. 1988; Moazzen-Ahmadi & McKellar 1993; Špirko et al. 1997), and has a band center at 2040.019 cm^{-1} (vacuum wavelength[1] 4.901915 μm; Krieg et al. 2013). The ν_3 mode of C_5 has also been investigated (Vala et al. 1989; Moazzen-Ahmadi et al. 1989; Massó et al. 2007) with a band center at 2169.442 cm^{-1} (4.609480 μm; Bernath et al. 1989). C_7 has yet to be detected in circumstellar envelopes, but the strongest vibrational band, the ν_4 antisymmetric stretch at 2138.314 cm^{-1} (4.676582 μm; Neubauer-Guenther et al. 2007), has been measured in the laboratory (Heath & Saykally 1991; Mogren Al-Mogren et al. 2013). The close proximity of these fundamental frequencies (within 0.3 μm) allow all three molecules to be studied in circumstellar shells using the same high-resolution instrument.

2 OBJECTS AND OBSERVATIONS

High-resolution infrared spectra were obtained of target carbon stars with known circumstellar shells using the 8.1 m Gemini South telescope and the NOAO Phoenix spectrometer (Hinkle et al. 1998). The observations (GS-2010A-Q-74) were carried out during the first half of 2010 and the program stars are listed in Table 1. All program stars are tip AGB Mira variables and their K band flux varies by approximately one magnitude. In addition to the program stars, a number of hotter reference stars were also observed for the removal of telluric features.

The Phoenix spectrometer is a cryogenically-cooled echelle spectrograph that uses order-separating filters to isolate individual echelle orders. The detector is a 1024×1024 InSb Aladdin II array. A 2 pixel slit width was used resulting in a spectral resolving power of $R = \lambda/\Delta\lambda \sim 70,000$. Three spectral regions were observed centred on 2045 cm^{-1} (4.890 μm), 2168 cm^{-1} (4.613 μm) and 2138 cm^{-1} (4.677 μm) to cover the corresponding C_3, C_5 and C_7 vibration bands. The size of the detector along the dispersion direction limits the wavelength coverage for a single observation to $\sim$0.5% ($\sim$10.5 cm^{-1} at 2100 cm^{-1}).

The observations and reductions employed standard thermal infrared techniques (Joyce 1992) and used the IRAF software package.[2] The spectra were wavelength calibrated using telluric lines of CO from HITRAN (Rothman et al. 2013) and a typical RMS uncertainty in the wavenumber scale is less than 0.005 cm^{-1}. The same HITRAN lines were used in the calculation of the telluric model atmospheres (see Section 3).

[1] All wavelegths are given for a vacuum.
[2] IRAF software is distributed by the National Optical Astronomy Observatories under contract with the National Science Foundation.

Table 1. Observations using the Phoenix Spectrometer on Gemini South (GS-2010A-Q-74)

Object	IRAS	Magnitude			Observation dates in 2010 (integration time in minutes)			Magnitude References
		J	*H*	*K*	C_3 Region	C_5 Region	C_7 Region	
Program Stars:								
CRL 865	06012 + 0726	–	11.3	7.7	24 Feb (24)	21 Feb (16)	23 Feb (32)	1
IRC +10216	09452 + 1330	7.3	4.0	1.2	03 Mar (0.8)	25 Feb (5.3)	23 Feb (8)	1
CRL 1922	17049 − 2440	12.2	9.2	6.3	12 Jun (8)	01 Mar (8)	26 Apr (16)	2
CRL 2023	17512 − 2548	13.2	9.5	6.5	12 Jun (16)	04 Mar (38)	22 May (32)	2
CRL 2178	18288 − 0837	11.7	8.0	5.2	–	23 May (52)	27 Jun (21.3)	2
CRL 3099	23257 + 1038	–	10.3	7.1	–	27 Jun (24)	–	1
Reference Stars:								
HIP 22509	04478 + 0848	4.26	4.21	4.17	–	21 Feb (16)	–	3, 4
HR 1790	05224 + 0618	2.17	2.24	2.32	24 Feb (38)	–	–	3
HR 2491	06429 − 1639	-1.36	-1.33	-1.35	–	25 Feb (2.7)	23 Feb (1.3)	3
HR 4662	12132 − 1715	2.76	2.83	2.81	12 Jun (50)	–	–	3
HR 5267	14002 − 6008	1.17	1.21	1.28	03 Mar (96)	01 Mar (48)	27 Jun (48)	4
HR 6553	17337 − 4258	1.07	0.87	0.84	–	04 Mar (24) 23 May (40) 27 Jun (53.3)	26 Apr (40) 22 May (40)	4

References. (1) Whitelock et al. (2006); (2) Chen & Yang (2012); (3) Ducati (2002); (4) Cutri et al. (2003).

3 MODEL ATMOSPHERES AND TELLURIC REMOVAL

The reference star observations, listed in Table 1, consistently have a lower signal-to-noise compared to the object spectra for which the typical signal-to-noise ratio is ∼500. When the reference spectra are used to correct for atmospheric absorption, the object spectra are degraded. Recently, Seifahrt et al. (2010) have demonstrated the advantage of using synthetically produced absorption atmospheric spectra to remove telluric features from spectra taken with the CRIRES spectrograph.

The Reference Forward Model[3] (RFM) is a line-by-line radiative transfer model used to calculate atmospheric transmission spectra and is often used to interpret satellite observations (Fischer et al. 2008). RFM can be used to compute the atmospheric transmission for an observer at any zenith angle, making RFM well suited to simulating astronomical reference spectra for telescope observations with differing airmass. The primary advantage of using RFM in place of the observed reference spectra is to eradicate noise introduced during the removal of telluric lines.

The synthetic spectra computed for this study were calculated using RFM v4.30, which uses the HITRAN 2012 database for molecular line parameters (Rothman et al. 2013). The Michelson Interferometer for Passive Atmospheric Sounding (MIPAS) night time model atmospheric profiles (*ngt.atm*) were used with the CO_2 profile scaled to 2010 concentrations and the H_2O profile scaled to match observation. A Gaussian instrument lineshape (FWHM = 0.03 cm^{-1}) was also used to account for the lineshape of the Phoenix spectrometer. In addition, telescope temperature measurements were combined with National Centers for Environmental Prediction (NCEP) temperature profiles for Gemini South during the period of measurement to adjust the temperature profile below 25 km (i.e., the troposphere and lower stratosphere). Above 25 km, the MIPAS *ngt.atm* temperature profile remained unchanged. Since the H_2O absorptions and weather conditions were different for each observation, it was necessary to produce an RFM synthetic spectrum for each program observation to replace the reference star observations.

The IRAF routine TELLURIC was used to remove telluric features and to ratio program stars with the RFM synthetic spectra. Figure 1 shows the observed C_3 spectral region (approximately 2041 − 2049 cm^{-1}) for IRC +10216 and the corresponding RFM synthetic spectrum, with strongly absorbing telluric features indicated. The resulting spectrum for IRC +10216

[3] Reference Forward Model, RFM (v4.30), A. Dudhia, University of Oxford, http://www.atm.ox.ac.uk/RFM

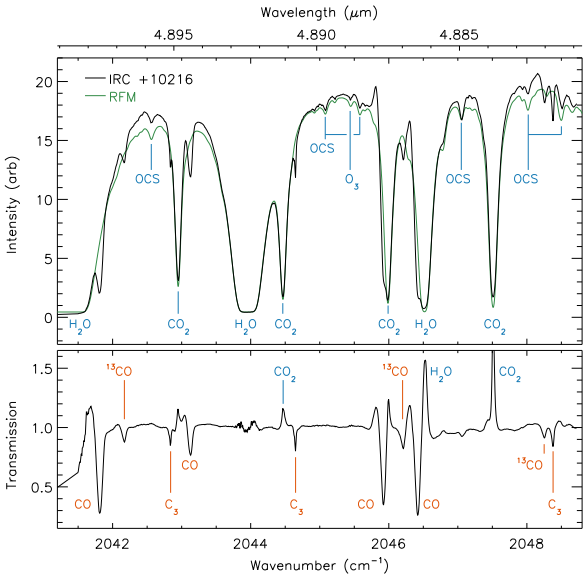

Figure 1. Calibrated spectrum of IRC +10216 with the corresponding RFM synthetic spectrum (upper panel) and resulting ratioed IRC +10216 spectrum with telluric lines removed (lower panel). Molecular absorption from telluric lines (blue) and the circumstellar shell (orange) have been indicated.

Table 2. Summary of C_3 line identifications

Program Star	Observed Lines[a] (cm^{-1})				Obs−Ref[b] (cm^{-1})	Temperature (K)	Partition Function	Column Density (cm^{-2})
	$R(2)$	$R(4)$	$R(6)$	$R(8)$				
CRL 865	2042.188	–	2045.845	2047.718	−0.480	44.3	40.3	9.6×10^{14}
IRC +10216	2042.835	2044.647	–	2048.377	+0.172	49.1	46.9	8.8×10^{14}
CRL 1922	2042.888	2044.670	–	2048.423	+0.222	29.3	24.8	6.8×10^{14}
CRL 2023	–	2044.714	–	2048.432	+0.233	50.0[c]	57.4	3.8×10^{14}

[a] in telluric frame of reference.
[b] average observed−reference (references determined from Krieg et al. 2013).
[c] estimated temperature.

is also shown in Figure 1 with circumstellar molecular lines identified. Whilst complete removal of some telluric features is not achieved (e.g., H_2O and CO_2), the result is an improvement on telluric removal when the reference star spectra are used. The C_3 absorptions are sharp and of moderate intensity (∼15% absorption) and can be identified before telluric features have been removed. The CO lines are unlike C_3 because they have characteristic P-Cygni profiles due to the distribution of CO throughout the circumstellar envelope at different radial velocities (Keady et al. 1988).

4 RESULTS

4.1 C_3

Telluric removal was carried out on all observations from Table 1 using RFM synthetic spectra. The observed C_3 spectral region contained the $R(2)$, $R(4)$, $R(6)$ and $R(8)$ rotational lines of the ν_3 antisymmetric stretch at 2042.66, 2044.48, 2046.32 and 2048.20 cm^{-1}, respectively. Table 2 summarises the line identifications for each of the program stars. Missing R-branch lines are due to absorption coincidences with telluric features due to relative velocity shifts. From these observations, the column densities and local standard of rest velocity shifts were calculated.

The ratioed program star spectra were normalised and the baseline was flattened to account for small variations over the

observed region. The C_3 absorption peaks were fit to a Gaussian lineshape using OriginPro 8.0. The rotational temperature of C_3 within the circumstellar envelope can be calculated from the relationship between the absorption intensity I, to temperature T (Herzberg 1989), since

$$I \propto (J' + J'' + 1)e^{-B''(J''+1)hc/kT}, \quad (1)$$

where $B'' = 0.436$ cm^{-1} (Krieg et al. 2013). The slope obtained from $\ln[I/(J' + J'' + 1)]$ versus $J''(J'' + 1)$ yields $-B''hc/kT$ and thus the temperature. The C_3 temperature for each program star is given in Table 2 based on the identification of each C_3 peak. For CRL 2023, only two lines were observed (giving a rotational temperature of 133 K) therefore an estimated temperature of 50 K was used instead.

The molecular C_3 column densities can be obtained from the Beer-Lambert law

$$I = I_0 e^{-S'g(\nu-\nu_{10})Nl}, \quad (2)$$

where S' is the 'line strength', I is the line intensity and $g(\nu - \nu_{10})$ is the line shape function (Bernath 2005). Integrating over the whole line and rearranging for column density Nl gives

$$Nl = \frac{1}{S'} \int \ln(I_0/I)d\nu, \quad (3)$$

where the integral is given by the area of each C_3 absorption peak and line strength, S', is obtained from

$$S' = \frac{2\pi^2 \nu_{10} S_{J'J''}}{3\epsilon_0 hcQ} e^{-E_0/kT}(1 - e^{h\nu/kT}). \quad (4)$$

The partition functions Q, was calculated individually for each program star (Table 2) based on the temperature and the contribution due to the rotational and vibrational components. The rotational line strength, $S_{J'J''}$, was calculated from the transition dipole moment $M_{\nu'\nu''}$ (Bernath 2005) as

$$S_{J'J''} = |M_{\nu'\nu''}|^2 \cdot \mathrm{HLF}, \quad (5)$$

where HLF is the Hönl-London Factor (HLF $= J'' + 1$ for R-branch lines of C_3) and $M_{\nu'\nu''} = 0.35$ debye (Jensen et al. 1992).

The spectral simulation program PGOPHER[4] was used to simulate the rotational spectrum of the ν_3 band of C_3 using the calculated temperature with the constants from Krieg et al. (2013). This provided the lower state energy, E_0, for each transition along with the rotational assignments.

From Equation 3, the average column densities of C_3 are calculated to be 9.6×10^{14}, 8.8×10^{14}, 6.8×10^{14} and 3.8×10^{14} cm^{-2} for CRL 865, IRC +10216, CRL 1922 and CRL 2023, respectively. These calculated column densities have an estimated error of 20% except CRL 2023, which is about a factor of two due to the estimated temperature. Figure 2 displays the $R(8)$ line of the ν_3 mode of C_3 for the program stars given in Table 2. The fitted Gaussian peak is displayed along with the area used to calculate the C_3 column density.

The sharp line shape of C_3 indicates that the molecule is contained within a narrow shell of each circumstellar envelope. Calibrating the spectra with telluric features determines the velocity shift (v_{obs}) of the observed line. The IRAF procedure RVCORRECT was used to calculate the velocity shifts due the motion of the Earth, Moon and Sun at the time of observation to provide the local standard of rest velocity (v_{lsr}). Comparing the v_{lsr} values to accepted stellar velocities (v_{obs}) for each object, the shell expansion velocity (v_{shell}) can be obtained from $v_{shell} = v_{lsr} - v_{obj}$; the results are summarised in Table 3.

4.2 C_5

A PGOPHER simulation of the ν_3 mode of C_5 at 50 K using the constants obtained from Moazzen-Ahmadi et al. (1989) and a band strength of 0.74 debye (Botschwina & Sebald 1989) predicts the $P(14)$ transition to be the most intense. Figure 3 displays the velocity shifted and ratioed spectrum for IRC +10216 in the proximity of the $P(14)$ transition, a number of small absorption features are coincident to the C_5 positions. There are tentative identifications of the $P(8)$, $P(10)$, $P(16)$ and $P(20)$ lines; the remaining lines are contaminated by telluric features and cannot be identified. The column density calculated from the strongest transition, $P(8)$, is 1.3×10^{13} cm^{-2}. This calculation has been carried out for the $P(8)$ transition in the spectra of the remaining objects observed in the C_5 region. These features are not as prominent as they are in IRC +10216 and the calculated column densities are estimated upper limits as summarised in Table 4.

[4] PGOPHER (v8.0.195), a program for simulating rotational structure, C. M. Western, University of Bristol, http://pgopher.chm.bris.ac.uk/

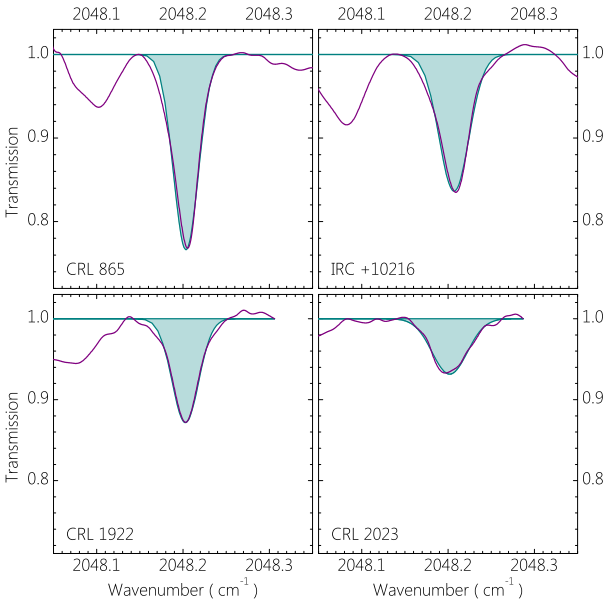

Figure 2. Calibrated identification of the $R(8)$ absorption line of the ν_3 mode of C_3 at 2048 cm^{-1} (4.882 μm) for observations in the circumstellar shells of CRL 865, IRC +10216, CRL 1922 and CRL 2023. The shaded region indicates the fitted area used to calculate the column density for each line.

Table 3. Velocity components (in km s^{-1}) for each program star from the velocity shifted C_3 absorptions

Object	Observed Velocity (v_{obs})	Local Standard of Velocity (v_{lsr})	Stellar Rest Velocity[a] (v_{obj})	Shell Velocity (v_{shell})
CRL 865	70.3	28.5	45.6	-17.1
IRC +10216	-25.2	-41.1	-23.2 (-26.0[b])	-17.9 (-15.1)
CRL 1922	-32.6	-22.6	-5.1	-17.5
CRL 2023	-34.1	-18.7	-	$\leqslant$ -18.7

[a] from Menzies et al. (2006).
[b] from Menten et al. (2012).

Table 4. Upper limit estimates for the C_5 column densities

Object	Column density upper limit[a] (cm^{-2})	Ratio[b]
CRL 2023	2.4×10^{12}	158
CRL 3099	5.1×10^{12}	–
CRL 865	9.4×10^{12}	102
CRL 2178	1.1×10^{13}	–
CRL 1922	1.2×10^{13}	57
IRC +10216	1.3×10^{13}	68

[a] except for IRC +10216.
[b] as C_3:C_5 column density.

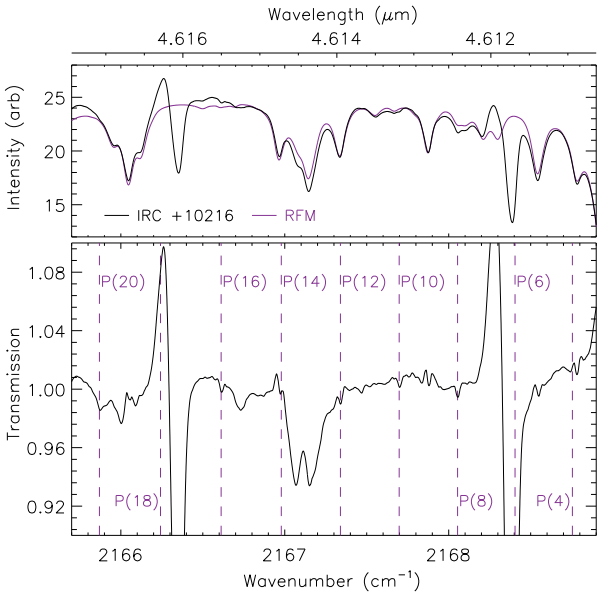

Figure 3. A section of the calibrated and velocity shifted spectrum of IRC +10216 and the corresponding RFM synthetic spectrum in the range of the ν_3 mode of C_5 (upper panel). The ratioed IRC +10216 spectrum highlights the position of the P-branch absorptions shown in purple (lower panel).

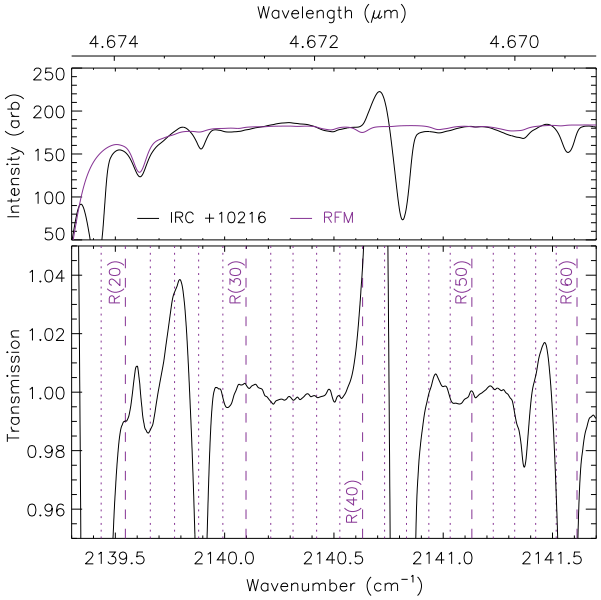

Figure 4. A section of the calibrated and velocity shifted spectrum of IRC +10216 and the corresponding RFM synthetic spectrum in the range of the ν_4 mode of C_7 (top panel). The R-branch line positions are shown in purple along with the ratioed IRC +10216 spectrum (lower panel).

4.3 C_7

A PGOPHER simulation of the ν_4 mode of C_7 at 50 K using the constants obtained from Neubauer-Guenther et al. (2007) and a band strength of 0.72 debye determined from a band intensity of 2809 km mol^{-1} (Kranze et al. 1996) predicts the $R(24)$ transition to be the most intense. Figure 4 displays the reduced spectrum for IRC +10216 with predicted C_7 line positions. No assignments can be made above the noise limit. The small 'peak' at 2140.12 cm^{-1} near $R(30)$ has been used to estimate an upper limit of the C_7 column density, assuming the molecule is contained within a shell at 50 K. The calculated upper limit for the C_7 column density in the circumstellar envelope of IRC +10216 is 4.7×10^{12} cm^{-2}.

Table 5. Summary of the observed and calculated column densities (in cm^{-2}) of small carbon chains in IRC +10216

Carbon chain	This work	Observed (Ref.)	Calculated (Ref.)
C_3	8.8×10^{14}	1.0×10^{15} (1)	2.0×10^{14} (4)
C_5	1.3×10^{13}	9.0×10^{13} (2)	2.0×10^{14} (4)
C_7	$\leqslant 4.7 \times 10^{12}$	$\leqslant 2.0 \times 10^{13}$ (3)	1.1×10^{14} (5)

References. (1) Hinkle et al. (1988); (2) Bernath et al. (1989); (3) Hinkle & Bernath (1993); (4) Li et al. (2014); (5) Millar et al. (2000).

5 DISCUSSION

Synthetic reference spectra were necessary due to the unsatisfactory noisy reference star spectra, which in some cases had noise close to 5%. We have demonstrated that line-by-line radiative transfer programs, such as RFM, are capable of creating suitable reference spectra for the removal of telluric features from obscured carbon stars in the infrared. These objects have complicated absorption spectra and a complete removal of telluric features is often difficult. Our synthetic spectra were created using a combination of measured and standard atmospheric conditions for the Gemini observatory. We restricted our adjustment of the standard RFM molecular atmospheric profiles to a scaling of the CO_2 and H_2O profiles. This kept the remaining molecular profiles consistent and accounts for differing humidity conditions during each observation. We also adjusted the standard temperature profile (which applies to all molecules) to coincide with the measured temperature at the telescope. For these reasons, the synthetic spectra do not completely remove telluric features, however it should be noted that this was also not possible (and worse) using the original reference star observations, most likely due to the fluctuating weather conditions during each observation run. Telescope time is a limited resource and is better spent on object acquisition, particularly if synthetic spectra are able to adequately simulate reference star observations.

The C_3 absorptions are clearly identifiable due to the strength of the ν_3 transition. They can be assigned before telluric removal (Figure 1) and were observed in the spectra of all program stars recorded in the C_3 region. These absorptions are underresolved at a resolution of 0.03 cm^{-1} and the sharp transitions are broadened by the instrument line shape function; resulting in a reduced absorption depth. Nevertheless, the calculated column density of 8.8×10^{14} cm^{-2} for C_3 in IRC +10216 compares very well to 1.0×10^{15} cm^{-2} obtained by Hinkle et al. (1988).

The same broadening occurs for our C_5 observations and a maximum absorption depth of ∼1% is seen. It was only possible to calculate the column density of C_5 in IRC +10216 by using a synthetic spectrum to remove the telluric lines. C_5 has previously been observed with a column density of 9.0×10^{13} cm^{-2} in the same spectral region of IRC +10216 by Bernath et al. (1989) using a high-resolution Fourier transform infrared spectrometer (0.01 cm^{-1} resolution); a maximum absorption depth of ∼3% was observed. The calculated value of 1.3×10^{13} cm^{-2} is approximately 15% of the value calculated by Bernath et al. (1989), however Botschwina & Sebald (1989) suggest that the Bernath et al. (1989) column density was an overestimate due to the transition dipole moment that was used. The C_5 transition dipole moment for this study was taken from Botschwina & Sebald (1989) and the column density presented here is within 25% of their estimated value of 5.0×10^{13} cm^{-2}.

The C_5 absorption lines for the remaining program stars (excluding IRC +10216) are at the noise limit when synthetic reference spectra are used. Therefore, it was only possible to provide an estimate of the upper limit for C_5 in these objects. Whilst these upper limits span almost one order of magnitude, and therefore should only be used as an indication, it is interesting to note a negative correlation between the column density of C_5 and the C_3:C_5 ratio.

Hinkle & Bernath (1993) have previously obtained an upper limit of 2.0×10^{13} cm^{-2} for a C_7 column density based on high-resolution spectra of IRC +10216. This work refines the column density upper limit for C_7 in IRC +10216 by almost one order of magnitude to 4.7×10^{12} cm^{-2}. The column densities of C_3, C_5 and C_7 are summarised and compared to previously determined and calculated values for IRC +10216 in Table 5.

The total empirical column density in IRC +10216 for neutral carbon is 1.1×10^{16} cm^{-2} (Keene et al. 1993) and for C_2 is 7.9×10^{14} cm^{-2} (Bakker et al. 1997). Figure 5 includes these values with those for C_3, C_5 and C_7 from this study and compares the empirical column densities to the number of carbon atoms. Also included in Figure 5 are calculated column densities for all pure carbon species from Millar et al. (2000) and the appropriate values from McElroy et al. (2013). Carbon

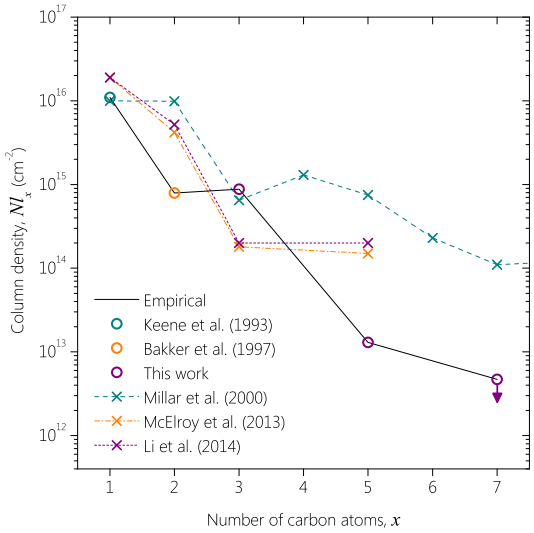

Figure 5. A comparison of the column densities of small carbon chain species in IRC +10216. Empirical column densities are shown by the solid black line and include the values for neutral carbon (Keene et al. 1993), C_2 (Bakker et al. 1997) and C_3, C_5 and C_7 from this work. The dashed lines refer to calculated column densities for IRC +10216 by Millar et al. (2000), McElroy et al. (2013) and Li et al. (2014).

chain column densities from a state-of-the-art model by Li et al. (2014), that improves the N_2 and CO photodissociation rates and shield functions of McElroy et al. (2013), is also shown.

The primary carbon chains growth pathways (Millar et al. 2000) are given by

$$C_2 + C_nH \rightarrow C_{n+2} + H$$

and

$$C_n^- + C_m \rightarrow C_{n+m}^- + h\nu \text{ leading to } C_{n+m}^- + h\nu \rightarrow C_{n+m} + e^-.$$

The latest models have reduced the column densities of C_3 and C_5, however there is still a disagreement between observation and calculation. Most notably, C_3 is underestimated whereas C_5 is overestimated. The calculated values from Millar et al. (2000), McElroy et al. (2013) and Li et al. (2014), shown in Figure 5, predict the column densities of C_3 and C_5 to be almost equal. Our work suggests that C_3 is almost 2 orders of magnitude greater than C_5 (see Table 5), which indicates a similar trend to that seen in Cherchneff & Glassgold (1993) where the abundance of C_3 was $\sim$10 times greater than C_5. The empirical column densities for small carbon chains (particularly C_2, C_3 and C_5) indicate that the reaction rates for small carbon chains in current models are incorrect; the models are missing important reactions; or the choice of initial circumstellar conditions is not suitable.

Carbon containing molecules are ubiquitous throughout the interstellar medium and are not confined to circumstellar envelopes (Herbst & van Dishoeck 2009). Linear carbon chain growth is thought to eventually lead to larger species like PAHs, cyanopolyynes, fullerenes and even amino acids. Benzene (C_6H_6) has been detected in proto-planetary nebula (Cernicharo et al. 2001), cyanopolyyne species containing a chain of as many as 11 carbon atoms ($HC_{11}N$) have been observed in dark interstellar clouds (Bell et al. 1997) and large fullerenes, such as C_{60} and C_{70}, have been observed in planetary nebula (Cami et al. 2010). Loison et al. (2014) consider a revised chemical model for dark interstellar clouds that includes a number of reactions that break down larger linear carbon chains into smaller chains via reaction pathways such as

$$C + C_n \rightarrow C_3 + C_{n-2},$$

where $n \leqslant 4$. They note that the consequence for linear carbon chains is to limit the abundance of longer chains ($C_{n>3}$) due to faster reaction rates, resulting in an accumulation of C_3, which has an estimated low reactivity. This would have the consequence of increasing the C_3 column density at the expense of C_5 (and longer chains), which would appear to improve current model calculations (Figure 5).

The C_3 column densities can be used to determine an average column density of 7.3×10^{14} cm^{-2} for the circumstellar envelopes of carbon-rich AGB stars. However, not all carbon stars have equivalent C/O ratios or mass loss rates, which are essential in understanding the circumstellar chemistry. The C/O ratio for IRC +10216 is given as 1.4 and the mass loss

rate has been calculated as $3.3 \times 10^{-5} M_{\odot}$ year^{-1} (Bergeat & Chevallier 2005), but these parameters are unavailable for the remaining objects so no correlations can be investigated. Since C_3 was observed in all objects, we believe IRC +10216 remains a prototypical example.

Bakker et al. (1997) identified a correlation between C_2 column densities and circumstellar expansion velocity. Our results show no correlation between C_3 or C_5 column densities with the shell velocity; however if the more recent stellar velocity of -26.0 km s^{-1} (Menten et al. 2012) is used for IRC +10216, a slight increase in column density is seen for decreasing shell velocity. Our velocities are consistent and indicate a typical circumstellar shell velocity to be approximately 17.5 km s^{-1}.

6 CONCLUSIONS

The small carbon chain C_3 has been detected in the circumstellar envelopes of CRL 865, IRC +10216, CRL 1922 and CRL 2023 by the identification of a number of vibration-rotation lines from the ν_3 antisymmetric stretch of C_3 near 2040 cm^{-1}. The calculated column densities are 9.6×10^{14}, 8.8×10^{14}, 6.8×10^{14} and 3.8×10^{14} cm^{-2}, respectively. We used synthetic spectra to remove telluric features from our observations, highlighting how a line-by-line radiative transfer model can be used to remove telluric features if reference star spectra are of poor quality or unavailable. C_5 was observed in IRC +10216 with a column density of 1.3×10^{13} cm^{-2}, and upper limits have been provided for 5 for other sources. An upper limit for the column density of C_7 in IRC +10216 was estimated to be 4.7×10^{12} cm^{-2}. Our measurements suggest a revision to circumstellar shell models may be needed to account for small carbon chain abundances.

ACKNOWLEDGMENTS

This work is based on observations obtained at the Gemini Observatory, which is operated by the Association of Universities for Research in Astronomy, Inc., under a cooperative agreement with the NSF on behalf of the Gemini partnership: the National Science Foundation (United States), the National Research Council (Canada), CONICYT (Chile), the Australian Research Council (Australia), Ministério da Ciência, Tecnologia e Inovação (Brazil) and Ministerio de Ciencia, Tecnología e Innovación Productiva (Argentina). Funding has been provided by a University of York studentship and Old Dominion University research fellowship, additional support was provided by the NASA laboratory astrophysics program. The authors would like to thank the reviewer's for their comments during the review process and Daniel Frohman for identifying appropriate band strengths to use in calculation of the C_5 and C_7 column densities.

REFERENCES

Ádámkovics M., Blake G. A., McCall, B. J., 2003, ApJ, 595, 235
Agúndez M., Cernicharo J., 2006, ApJ, 650, 374
Agúndez M., Fonfría J. P., Cernicharo J., Kahane C., Daniel F., Guélin M., 2012, A&A, 543, A48
Bakker E. J., van Dishoeck E. F., Waters L. B. F. M., Schoenmaker T., 1997, A&A, 323, 469
Baronavski A. P., McDonald J. R., 1977, J. Chem. Phys., 66, 3300
Bell M. B., Feldman P. A., Travers M. J., McCarthy M. C., Gottlieb C. A., Thaddeus P., 1997, ApJ, 483, L61
Bergeat J., Chevallier L., 2005, A&A, 429, 235
Bernath P. F., Hinkle K. H., Keady J. J., 1989, Science, 244, 562
Bernath P.F., 2005, Spectra of Atoms and Molecules (Second Edition), Oxford University Press, New York, USA
Botschwina P., Sebald, P., 1989, Chem. Phys. Lett., 160, 485
Cami J., Bernard-Salas J., Peeters E., Malek S. E., 2010, Science, 329, 1180
Cernicharo J., Goicoechea J. R., Caux E., 2000, ApJ, 534, L199
Cernicharo J., Heras A. M., Tielens A. G. G. M., Pardo J. R., Herpin F., Guélin M., Waters L. B. F. M, 2001, ApJ, 546, L123
Cernicharo J., et al., 2010, A&A, 521, L8
Cernicharo J., Agúndez M., Guélin M., 2011, in Cernicharo J., Bachiller R., eds., IAU Symp. 280, The Molecular Universe. Cambridge Univ. Press, Cambridge, p. 237
Chen P. S., Yang X. H., 2012, AJ, 143, 36
Cherchneff I., Glassgold A. E., 1993, ApJ, 419, L41

Cherchneff I., 2006, A&A, 456, 1001
Cherchneff I., 2012, A&A, 545, A12
Crampton D., Cowley A. P., Humphreys R. M., 1975, ApJ, 198, L135
Cutri R. M., et al., 2003, VizieR Online Data Catalog, 2246, 0
Ducati J. R., 2002, VizieR Online Data Catalog, 2237, 0
Ehrenfreund P., Charnley S. B., 2000, ARA&A, 38, 427
Fischer H., et al., 2008, Atmos. Chem. Phys., 8, 2151
Glassgold A. E., 1996, ARA&A, 34, 241
Goulay F., Nemes L., Schrader P. E., Michelsen H. A., 2010, Mol. Phys., 108, 1013
Heath J. R., Saykally R. J., 1991, J. Chem. Phys., 94, 1724
Herbst E., van Dishoeck E. F., 2009, ARA&A, 47, 427
Herzburg G., 1989, Molecular Spectra and Molecular Structure: I. Spectra of Diatomic Molecules, Krieger Publishing Company, Florida, USA
Hinkle K. W., Keady J. J., Bernath, P. F., 1988, Science, 241, 1319
Hinkle K. H., Bernath, P. F., 1993, in Kwok S., eds., Atronom. Soc. Pac. Conf. Proc, 41, Astronomical Infrared Spectroscopy: Future Observational Directions. PASP, San Francisco, p. 125
Hinkle K. H., Cuberly R. W., Gaughan N. A., Heynssens J. B., Joyce R. R., Ridgeway S. T., Schmitt P., Simmons J. E., 1998, in Fowler A. M., ed., Proc. SPIE Conf. Ser. 3354, Infrared Astronomical Instrumentation. SPIE, Bellingham, p. 810
Joyce R. R., 1992, in Howell S., ed., Atronom. Soc. Pac. Conf. Ser. 23, Astronomical CCD Observing and Reduction Techniques. PASP, San Francisco, p. 258
Jensen P., Rohlfing C. M., Almloef J., 1992, J. Chem. Phys., 97, 3399
Kaiser R. I., 2002, Chem. Rev., 102, 1309
Keady J. J., Hall D. N. B., Ridgway S. T., 1988, ApJ, 326, 832
Keene J., Young K., Phillips T. G., Buettgenbach T. H., Carlstrom, J. E., 1993, ApJ, 415, L131
Kranze R. H., Rittby C. M. L., Graham, W. R. M., 1996, J. Chem. Phys., 105, 5313
Krieg J., et al., 2013, J. Phys. Chem. A, 117, 3332
Li X., Millar T. J., Walsh C., Heays A. N., van Dishoeck, E. F., 2014, preprint (arXiv:1406.7354)
Loison J.-C., Wakelam V., Hickson K. M., Bergeat A., Mereau, R., 2014, MNRAS, 437, 930
McElroy D., Walsh C., Markwick A. J., Cordiner M. A., Smith K., Millar T. J., 2013, A&A, 550, A36
Massó H., Veryazov V., Malmqvist P.-Å., Roos B. O., Senent M. L., 2007, J. Chem. Phys., 127, 154318
Matsumura K., Kanamori H., Kawaguchi K., Hirota E., 1988, J. Chem. Phys., 89, 3491
Menten K. M., Reid M. J., Kamiński T., Claussen M. J., 2012, A&A, 543, A73
Menzies J. W., Feast M. W., Whitelock P. A., 2006, MNRAS, 369, 783
Millar T. J., Herbst E., Bettens R. P. A., 2000, MNRAS, 316, 195
Moazzen-Ahmadi N., McKellar A. R. W., Amano T., 1989, J. Chem. Phys., 91, 2140
Moazzen-Ahmadi N., McKellar A. R. W., 1993, J. Chem. Phys., 98, 7757
Mogren Al-Mogren M., Senent M. L., Hochlaf M., 2013, J. Chem. Phys., 139, 064301
Mookerjea B., et al., 2012, A&A 546, A75
Neubauer-Guenther P., Giesen T. F., Schlemmer S., Yamada K. M. T., 2007, J. Chem. Phys., 127, 014313
Olofsson H., 2008, Physica Scripta Vol. T, 133, 014028
Rothman L. S., et al., 2013, J. Quant. Spectrosc. Radiat. Transfer, 130, 4
Seifahrt A., Käufl H. U., Zängl G., Bean J. L., Richter M. J., Siebenmorgen R., 2010, A&A, 524, A11
Souza S. P., Lutz B. L., 1977, ApJ, 216, L49
Špirko V., Mengel M., Jensen P., 1997, J. Mol. Spectrosc., 183, 129
Tsuji T., 1973, A&A, 23, 411
Vala M., Chandrasekhar T. M., Szczepanski J., van Zee R., Weltner Jr. W., 1989, J. Chem. Phys., 90, 595
Whitelock P. A., Feast M. W., Marang F., Groenewegen M. A. T., 2006, MNRAS, 369, 751
Zhang Y., Kwok S., Dinh-V-Trung, 2009, ApJ, 691, 1660
Zhang Y., Kwok S., Nakashima, J.-i., 2009, ApJ, 700, 1262
Ziurys L. M. 2006, Proc. Natl. Acad. Sci., 103, 12274

This paper has been typeset from a TEX/ LATEX file prepared by the author.